CFD Simulation of gas-solid flow during steam reforming of glycerol in a fluidised bed reactor

Binlin Dou; Valerie Dupont *; Paul T. Williams

Energy & Resources Research Institute, University of Leeds, Leeds, LS2 9JT, UK

Corresponding author: V.Dupont@leeds.ac.uk

Abstract: A CFD simulation of gas-solid flow in a fluidised bed reactor was performed to investigate the steam reforming of glycerol using a three-step reaction scheme, motivated by the worldwide increase of crude glycerol produced by the transesterification of vegetable oil into biodiesel. The Eulerian–Eulerian two-fluid approach was adopted to simulate hydrodynamics of fluidisation, and chemical reactions were modelled by the laminar finite-rate model. The gas-solid system exhibited a more heterogeneous structure. Clusters were observed to fall and stack together along the wall, and the process of wall slug formation was very evident. This suggests the bed should be agitated to maintain satisfactory fluidising conditions. The results showed that the glycerol conversion increased with increasing reaction time and most of the gas products H_2, CO_2, CH_4 and CO were formed during the initial 2 s. The prediction of the gas-solid phase flows and mixing, glycerol conversion and products distribution will provide helpful data to design and operate a bench scale catalytic fluidised bed reactor.

Keywords: CFD; Simulation; Glycerol; Steam reforming; Fluidised-bed reactor

---

*, Author to whom correspondence should be addressed. Tel: 44 -113-3432503; Fax: 44 -113-2467310, v.dupont@leeds.ac.uk.

1. Introduction

The steam reforming of glycerol for hydrogen production in a fluidised bed reactor involves some complex flows and reactions. Crude glycerol is a significant by-product of the transesterification of vegetable oil to fatty acid methyl esters (biodiesel), a process which is undergoing a boom through the building of new bio-refineries worldwide as part of the global efforts to combat climate change and reduce dependency on fossil fuel imports.[1] The successful design and operation of hydrogen production from glycerol depends on an ability to predict the behaviour in the system, especially the hydrodynamics, mixing of individual phases, mass transfer and multiple chemical reactions. An experimental approach to directly measure the behaviour is quite a difficult technique and carries the penalty of a high cost of operation. Accordingly, a Computational Fluid Dynamics (CFD) modelling can provide a powerful tool to investigate more economically the detailed flow phenomena and predict reaction conversion and hydrogen production. The purpose of this study was to estimate the hydrogen production from the steam reforming of glycerol, and to use the hydrodynamics information and reaction kinetics to predict the performance of a fluidised bed reactor.

The method of the gas-solid fluidized bed reactor has a number of unusual characteristics including the flowing continuity and rapid mixing of the solid particles, which leads to the intensity of the heat transfer and nearly isothermal conditions throughout the reactor; hence operation can be controlled smoothly and reliably. It is suited to large-scale industrial operations. Reactions in a fluidised bed reactor usually use fine solids that have a very small minimum fluidising velocity as bubbling bed, and early models of the dense bubbling fluidised bed reactor were generally based on the two-phase concept of fluidisation, originally proposed by Toomey and Johnstone,

which assumed that all gas in excess of that required for incipient fluidisation passed through the bed as bubbles.[2,3] The general two-phase model has been adapted to simulate the hydrodynamics in the catalytic fluidised bed reactor.[4~6] The significant research efforts have also been made to study the cluster formation and core-annular flow, which was experimentally observed in the riser flows of fluidised bed reactor.[7~10] The granular kinetic theory using an early version of the commercial simulation software FLUENT by Benyahia et al. has been presented as part of their efforts in the simulations of dilute-phase riser flow.[11] Some researchers have investigated the hydrodynamics and reaction kinetics of the gas-solid fluidised beds containing the fluid catalytic cracking particles by CFD simulation to ozone decomposition following a first-order reaction kinetics.[12,13]

2. Numerical simulation

2.1 Numerical method

The fluidising regime in a fluidised bed reactor can be simulated by: the Eulerian–Eulerian two-fluid model and the Eulerian–Lagrangian trajectory model. The gas and particle phases in the two-fluid model are both assumed to be continuous and solved in Eulerian coordinate, whereas with the trajectory model, the gas is considered as the continuous medium and the particle is treated with the Lagrangian coordinates by solving the equation of motion.[14,15]

In this paper, an Eulerian–Eulerian two-fluid approach with species transport is adopted to simulate the gas-solid flow and reactions. The chemical mechanism is modelled by the laminar finite-rate model, which computed the chemical source terms using Arrhenius expressions.[16] Solid shear and bulk viscosity within the reactor are

described using the kinetic theory of granular flow. The standard FLUENT code version 6.3 was used to carry out the modelling.

2.2 Gas-solid flow equations

The gas-solid flow prediction in the riser of fluidised bed was obtained by numerical solution of the conservation equations for the gas and particle phases. The continuity for phase q (q=g for gas phase and s for solid phase) is:[3,6-14,16,17]

$$\frac{\partial}{\partial t}(\varepsilon_q \rho_q) + \nabla \cdot (\varepsilon_q \rho_q \vec{v}_q) = 0 \tag{1}$$

where ε is the fraction of each phases, $\vec{v}$ is the velocity vector, and ρ is the density.

with the constraint:[6,7,13]

$$\sum \varepsilon_q = 1 \tag{2}$$

The conservation of momentum for the gas phase:[6,11-14,16,17]

$$\frac{\partial}{\partial t}(\varepsilon_g \rho_g \vec{v}_g) + \nabla \cdot (\varepsilon_g \rho_g \vec{v}_g \vec{v}_g) = -\varepsilon_g \nabla p + \nabla \bar{\tau}_g - K_{gs}(\vec{v}_g - \vec{v}_s) + \rho_g \varepsilon_g \vec{g} \tag{3}$$

where $\vec{g}$ is the gravity acceleration, p is the thermodynamic pressure, K_{gs} is the interface momentum transfer coefficient, and $\bar{\tau}_g$ is the viscous stress tensor of gas phase.

The conservation of momentum for the solid phase:[3,6,13]

$$\frac{\partial}{\partial t}(\varepsilon_s \rho_s \vec{v}_s) + \nabla \cdot (\varepsilon_s \rho_s \vec{v}_s \vec{v}_s) = -\varepsilon_s \nabla p - \nabla p_s + \nabla \bar{\tau}_s - K_{gs}(\vec{v}_s - \vec{v}_g) + \rho_s \varepsilon_s \vec{g} \tag{4}$$

where $\bar{\tau}_s$ is the solids stress tensor and p_s is the solids pressure.

The conservation of the kinetic energy of the moving particles is described as follows by the granular temperature, Θ_s :[11-14,16]

$$\frac{3}{2}[\frac{\partial}{\partial t}(\varepsilon_s\rho_s\Theta_s)+\nabla\cdot(\varepsilon_s\rho_s\vec{v}_s\Theta_s)]=(-p_s\bar{I}+\bar{\tau}_s):\nabla\vec{v}_s+\nabla\cdot(k_s\nabla\Theta_s)-\gamma_s+\phi_{gs} \quad (5)$$

The solid pressure, p_s is expressed as:[3,6,11,13]

$$p_s=\rho_s\varepsilon_s\Theta_s+2\rho_s(1+e)\varepsilon_s^2 g_0\Theta_s \quad (6)$$

where e is the restitution coefficient and g_0 is the radial distribution function given by:[3-13,16,17]

$$g_0=\frac{3}{5}[1-(\frac{\varepsilon_s}{\varepsilon_{s,max}})^{1/3}]^{-1} \quad (7)$$

The momentum exchange between the gas and solid phases is expressed by the drag coefficient repeated by an interphase exchange coefficient. The drag law of Gidaspow, which is a combination of the Wen and Yu model for dilute flow and Ergun equation for dense phase, was used for the gas-solid interphase exchange coefficient, K_{gs}. If $\varepsilon_s > 0.8$, K_{gs} is calculated with the equation from the Wen and Yu model as:[6,11-13]

$$K_{gs}=\frac{3}{4}C_D\frac{\varepsilon_s\varepsilon_g\rho_g|\vec{v}_g-\vec{v}_s|}{d_s}\varepsilon_g^{-2.65}$$

(8)

The C_D is the drag coefficient, is expressed as:[3,7,11-13]

$$C_D=\begin{cases}\frac{24}{Re}(1+0.15\,Re)^{0.687}, Re<1000 \\ 0.44, Re\geq1000\end{cases}$$

(9)

And the Reynolds number is calculated:

$$Re=\frac{\rho_g d_s|\vec{v}_g-\vec{v}_s|}{\mu_g} \quad (10)$$

If $\varepsilon_s \leq 0.8$, K_{gs} is calculated with the equation from the Ergun equation for dense

phase model as:[11, 13]

$$K_{gs} = 150 \frac{\varepsilon_s^2 \mu_g}{\varepsilon_g d_s^2} + 1.75 \frac{\varepsilon_s \varepsilon_g \rho_g |\vec{v}_g - \vec{v}_s|}{d_s} \tag{11}$$

The stress tensors for both gas and solid phases, $\bar{\tau}_g$ and $\bar{\tau}_s$ are expressed by:[13]

$$\bar{\tau}_g = \varepsilon_g \mu_g (\nabla \vec{v}_g + \nabla \vec{v}_g^T) \tag{12}$$

$$\bar{\tau}_s = 2\varepsilon_s \mu_s (\nabla \vec{v}_s + \nabla \vec{v}_s^T) + \varepsilon_s (\lambda_s - \frac{2}{3}\mu_s)\nabla \vec{v}_s \bar{I} \tag{13}$$

The solids shear viscosity was chosen to be expressed as:[7,11]

$$\mu_s = \frac{2\mu_{s,dil}}{(1+e)g_0}[1 + \frac{4}{5}g_0\varepsilon_s(1+e)]^2 + \frac{4}{5}\varepsilon_s \rho_s d_s(1+e)g_0(\frac{\Theta_s}{\pi})^{1/2}$$

(14)

The solid phase dilute viscosity in eq.14 is expressed by:[7,11]

$$\mu_{s.dil} = \frac{5\rho_s d_s \sqrt{\Theta_s \pi}}{96}$$

(15)

The solids bulk viscosity is expressed by:[7,11-13]

$$\lambda_s = \frac{4}{3}\varepsilon_s \rho_s d_s g_0(1+e)(\frac{\Theta_s}{\pi})^{1/2}$$

(16)

The diffusion coefficient for granular energy, k_s is expressed by the Gidaspow model:[3,11-13]

$$k_s = \frac{150\rho_s d_s \sqrt{\Theta_s \pi}}{384(1+e)g_0}[1 + \frac{6}{5}\varepsilon_s g_0(1+e)]^2 + 2\rho_s d_s \varepsilon_s^2 g_0(1+e)\sqrt{\frac{\Theta_s}{\pi}}$$

(17)

The collision dissipation of energy, γ_s is calculated from:[7,11-13]

$$\gamma_s = \frac{12(1-e^2)g_0}{d_s\sqrt{\pi}}\rho_s\varepsilon_s^{\,2}\Theta_s^{\,2/3}$$

(18)

The transfer of kinetic energy, ϕ_{gs} is expressed as:[11-13]

$$\phi_{gs} = -3K_{gs}\Theta_s$$

(19)

2.3 Fluidising regime

When a particle of size d_s falls through a fluid, its terminal free-fall velocity, v_s can be estimated from fluid mechanics by the expression:[2,3]

$$v_s = [\frac{4d_s(\rho_s - \rho_g)g}{3\rho_g C_D}]^{1/2}$$

(20)

The minimum fluidized velocity can be obtained as:[18]

$$v_{mf} = \frac{\mathrm{Re}_{mf}\,\mu_g}{d_p\rho_g}$$

(21)

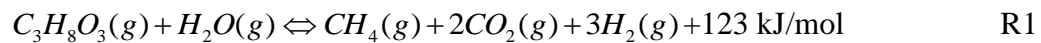where $\mathrm{Re}_{mf} = (\sqrt{27.2^2 + 0.0408A_r} - 27.2)$

(22)

and the Archimedes number, A_r, is defined as:[18]

$$A_r = \frac{\rho_g(\rho_s - \rho_g)gd_s^3}{\mu_g^2}$$

(23)

2.4 Reaction kinetics

The steam reforming of glycerol derived from biomass is a complex set of elementary steps that involve several intermediates and where many reaction pathways are possible, depending on the catalyst and reaction conditions. The main reaction mechanism comprises dehydrogenation or dehydration routes. Methane produced as intermediate product can further undergo the steam reforming reaction generating hydrogen and carbon monoxide.[19,20] Some studies indicated that the total quantity of coke formed on the catalyst decreased with increasing temperature and was almost negligible at above 600°C.[19-21] In this study, we did not consider the reactions of coke formation, thus simplifying model and shortening computing times. The following reactions were included in the CFD model in order to examine the fluidised bed reaction kinetics:

$$C_3H_8O_3(g) + H_2O(g) \Leftrightarrow CH_4(g) + 2CO_2(g) + 3H_2(g) + 123 \text{ kJ/mol} \qquad \text{R1}$$

$$CH_4(g) + H_2O(g) \Leftrightarrow CO(g) + 3H_2(g) + 206 \text{ kJ/mol} \qquad \text{R2}$$

$$CO(g) + H_2O(g) \Leftrightarrow CO_2(g) + H_2(g) - 41 \text{ kJ/mol} \qquad \text{R3}$$

The overall reaction of hydrogen production from glycerol steam reform can be written as:

$$C_3H_8O_3(g) + 3H_2O(g) \Leftrightarrow 3CO_2(g) + 7H_2(g) + 345 \text{ kJ/mol} \qquad \text{R4}$$
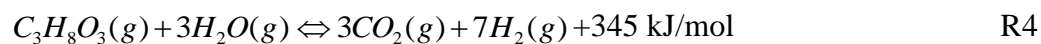
The reactions are assumed to occur in the entire riser section, and the flowing transport equation is included to predict the local mass fraction of each species, X_i:[16]

$$\frac{\partial(\rho_i X_i)}{\partial t} + \nabla \cdot (\rho_i \vec{v}_i X_i) = -\nabla J_i + R_i$$

(24)

J_i is the diffusion flux of species i, written as:[16]

$$J_i = -\rho_i D_i \nabla X_i$$

(25)

where D_i is the diffusion coefficient for species i in the mixture.

The source of chemical species i due to reaction, R_i, is computed as the sum of the reaction source over the N_R reactions using Arrhenius expressions.[16]

2.5 System setup and simulation parameters

The simulated fluidised bed was 1.0 m tall and 0.30 m wide. The grid was created in a CAD program called GAMBIT and exported into simulation software FLUENT. Figure 1 shows the two-dimensional computational domain of the fluidised bed reactor described by 8512 cells, 17212 faces and 8701 nodes. The initial bed was packed with granular solids of sand and catalyst with a volume fraction of 0.52. The granular phase had a single density and a single particle size to reduce the computational effort. The N_2 was as the carrier gas and fluidization gas, also to dilute the glycerol concentration in the system. The gas phase of isothermal mixtures with no phase exchange included the gases of glycerol, steam and N_2. The inlet molar concentrations were set at 1.10×10^{-3}, 6.22×10^{-3}, and 3.24×10^{-2} kmol/m^3 for glycerol, steam and N_2, respectively. With these conditions, the ratio of inlet glycerol concentration to inlet total gas concentration is 2.8% (vol.)

The gas phase at the wall was described by a no-slip boundary condition. The initial solid normal velocity was set at zero and the reactor was assumed in isothermal conditions throughout the reactor at 600°C. Due to the relatively low pressure drop in the system, the gas phase was assumed incompressible, an assumption further aided by the large N_2 dilution and isothermal conditions used here. Thus the pressure did not need to be defined at the inlet but outlet pressure was specified. The CFD model did not include any kinds of heat transfer. The inputs of time step of 0.001 s with 40 iterations per time step were chosen. The convection terms were described using

second-order upwind discretisation schemes. The parameter values used in this simulation are shown in Table 1.

3. Results and discussion

3.1. Fluidisation Hydrodynamics

Bed expansion and the existence of clusters, which greatly change the interaction of the gas phase and the particle phase, play a significant role in the fluidised bed reactor. In general, observation of bed expansion is based on the fluidised bed height and the initial bed height, when solids concentration is significantly higher than the local time-mean solids concentration it is indicated that most particles gather into clusters. The average particle height, $\bar{h}_p$ can be defined to characterise the bed expansion as:[9]

$$\bar{h}_p = \frac{\sum_c^{N_{cells}} \varepsilon_{s,c} h_c}{\sum_c^{N_{cells}} \varepsilon_{s,c}}$$

(26)

where c represents the cell, N represents the cells number, $\varepsilon_{s,c}$ is the average solids fraction and h_c is the particle height.

In this study, v_{mf} was estimated as 0.05 m/s and the development of the gas-solid fluidisation is illustrated during the first 4 s of the simulation. Figure 2 shows that the simulation results of the solids volume fraction using the Gidaspow drag law. The averaged particle height was computed after 1.5 s to avoid initial transient fluctuations. The values of the averaged particle heights were estimated as 0.37-0.42 m, indicating the bed expansion was about 300%-350%.

It can be seen, the gas-solid system exhibited a more heterogeneous structure, the dense phase developed into a uniform structure characterised by maximum volume fraction of 0.52, with particles clusters forming and dissolving dynamically. The process of wall slug formation was very evident. Clusters could be observed to fall along the wall, stack together and then protrude from the wall, while particles were dynamically squeezed out of these clusters and pushed upward by the up-flowing gas, and then these particles further aggregated into strands at an upper section of the bed.

When no collisions occur, the forces acting on the particles movement are mainly drag force ($\vec{F}_g$) and gravity ($m\vec{g}$):[8,15]

$$m\frac{d\vec{v}_s}{dt} = \vec{F}_g + m\vec{g}$$

(27)

In terms of the laws of classical physics, when two spherical particles move in opposite directions and impact each other, elastic deformation at the contact point occurs. The extent of deformation depends on the relative velocity of the particles and their stiffness. The particles are subjected to an elastic resistance after the collision in their original direction of motion. The resistance force is directly proportional to the displacement of the deformation and the stiffness of the particle material. When the displacement reaches a maximum value, the particles cease forward motion and rebound along the original direction. If particle collisions are not completely elastic, then some kinetic energy will be lost upon impact. The magnitude of the loss is related to the damping coefficient and the relative velocity of the particles. When a non-central collision occurs, a tangential torque appears because of the tangential

force. This tangential torque enables the particles to rotate. The velocity of solid particle after the collision can be expressed as:[15]

$$\vec{v}_s^{\,/} = \vec{v}_s + \vec{a}\nabla t$$

(28)

where $\vec{a}$ is the acceleration, and ∇t is the time step.

The cluster formation, which may involve gas-particle, particle-particle and particle-wall interactions, is too complex to be well understood. The gas bubble is an important phenomenon, some bubbles are produced which not only move upward, but also move transversely. Particle clusters were dragged to move transversely following the bubbles. The bubbles movement, their bursting and their size changes are the main factors affecting particles circulation and clusters formation, resulting in gas-solid phase transfer and reaction.

Figures 3 and 4 present the solid and gas velocities predicted by the CFD model, respectively. As can been seen, the internal circulation of particles occurred, and the gas was not very distributed evenly. The core-annulus structure shows that the solid and gas velocities in the core region are much higher than those in the annulus region, while solid and gas velocities near the wall are decreasing and downward, this may lead to the back mixing and internal circulation behaviour. Overall the flow and mixing structure seemed rather heterogeneous. Similar results have been obtained by other researchers.[9,17]

The pressure drop variation across the bed is mainly due to the two-phase interaction and fluidisation conditions. In a conventional fluidised bed, the pressure drop through the bed is just equal to the weight of the solids in the bed.[22] Some researchers stated that the total pressure drop per unit length along the riser included four main components:[22]

$$\left(\frac{dP}{dz}\right)_{total} = \left(\frac{dP}{dz}\right)_s + \left(\frac{dP}{dz}\right)_{acc} + \left(\frac{dP}{dz}\right)_{fs} + \left(\frac{dP}{dz}\right)_{fg}$$

(29)

where $(dP/dz)_s$ is the pressure drop due to the hydrodynamic head of solids, $(dP/dz)_{acc}$ is the pressure drop due to solids acceleration, $(dP/dz)_{fs}$ and $(dP/dz)_{fg}$ are the pressure drops due to solids and gas frictions, respectively. An expression of pressure drop across the bed can be given as:[10]

$$\Delta P = (\rho_s - \rho_g)(1 - \varepsilon_{mf})gL$$

(30)

where L is the height of the bed, and ε_{mf} is the bed void fraction at minimum fluidization. In general, the exact value of ε_{mf} can be measured experimentally, the value from 0.40 to 0.50 for ε_{mf} should be a reasonable range based on the studied bed.[2,3] Figure 5 showed the values of the pressure drop in initial time of 4 s. A considerable pressure fluctuation with time was observed and the predicted values by eq.36 were close to the values by CFD simulation. The prediction of pressure drop in the fluidised bed reactor is a problem of long standing interest in the industry.[20] In fact, when fluidising slugging occurs; it is very difficult to give a precise prediction of pressure drop by theoretical expressions.

3.2 Glycerol conversion and hydrogen production

To perform the predictions of glycerol conversion and hydrogen production in this study, three main reactions included in the CFD model followed first-order reaction kinetics without considering the reverse reactions because effect of the reverse reactions of R1, and R2 on hydrogen production in glycerol steam reforming is negligible at 600°C. At this temperature, the reverse water gas shift (R3$_r$) is active

but its effects can still be neglected without largely affecting the results. The performance of reactor is presented in terms of glycerol and steam conversions and H_2, CO_2, CH_4 and CO selectivity. The glycerol and steam conversions were calculated by the molar flow rates of glycerol and steam at inlet and outlet, defined as:

$$Conv_i(\%) = 100 \times \frac{(N_k x_i v_i)_{inlet} - \sum_{1}^{N_k}(x_i v_i)_{outlet}}{(N_k x_i v_i)_{inlet}}$$

(31)

where N_k represents the computed cell number at inlet, x_i represents the molar fraction of species i, and i represents the glycerol or steam.

The products selectivity was calculated by the following definitions:

$$H_2, Selectivity(\%) = 100 \times \frac{2n_{H2,out}}{2(n_{H2O,in} - n_{H2O,out}) + conv_{glycerol} \times 8n_{glycerol,in}}$$

(32)

i, $Selectivity(\%) = 100 \times (C$ atoms in species i $)/(C$ atoms produced in gas phase$)$

(33)

where n represents the average molar flow rate, kmol/s; and species i = CO_2, CH_4 and CO.

An increase in glycerol conversion from 22% at 1s to 45% at 4 s, and plateauing with increasing time, is shown in Figure 6. Concentrations of the products H_2, CO_2, CH_4, and CO at the outlet with time are plotted in Figure 7. Most gas products were shown to form during the initial 2 s. The concentration of CO was negligible and is shown on a smaller scale than the rest of the products. It was seen to increase greatly with increasing the time when the CH_4 reforming reaction took place. Steam conversion was in the 20% range after 1s. A fluctuation of seam conversion with time was observed in

this simulation. In practical process of glycerol steam reforming, the product gases may include the steam produced by glycerol decomposition. On the basis of these data, the calculated selectivity of gas products and the mole ratio of H_2/CO_2 are shown in Figure 8. Apart from the H_2 product, CO_2 and CH_4 remained in significant quantities and selectivity, which indicated reaction R1 converted glycerol easily to CO_2 and CH_4. Some studies indicated that glycerol decomposition to CH_4 and CO_2 is highly favourable during the steam reforming process.[21] The increases in the product concentrations of H_2, CO_2, CH_4 and CO were mainly due to the increase in glycerol conversion. H_2 selectivity increased with time and no significant changes were found in CO_2 and CH_4 selectivity. Water gas shift reaction of CO (R3) produces CO_2 and decreases CO selectivity. Methane reforming (R2) can result in decreasing the CO selectivity. Very low CO selectivity observed in Fig. 8 was partially due to effects of methane reforming (R2) and water gas shift reaction (R3), and the mole ratio of H_2/CO_2 as main product gases kept a constant value in the initial times. Figure 9 shows the CFD-simulated distribution of glycerol and of the products concentrations at 4 s. Most of the glycerol conversion and product formation occurred in the middle of the bed and increased downstream. This can be attributed to differences of the reaction rates. Fig. 10 gives the distributions of Arrhenius rates for three chemical reactions at 4 s and the highest values of the rates for R1 and R2, 3 were 3.27×10^{-4} and 6.55×10^{-7} kmol/m^3·s, respectively. The results showed the rate of R1 was greatly higher than others, which indicated that the chemical reaction of R1 with CH_4 product dominated the process in initial reaction times, and obviously CH_4 was not a

desirable product. Some investigations indicated that the concentration of CH_4 decreased with increasing reaction temperature in the methane steam reforming.[20,23,24]

Gas-solid flow and reaction models developed for simple patterns can be extended to deal with the more complex problems normally encountered in industry. In the present study, the implementation of an additional transport equation with a kinetic term in the CFD model predicted the production process of hydrogen and the simulated glycerol conversion and products distribution. The latter provides helpful data to design the catalytic fluidised bed reactor. As can be seen from the results of this simulation, the conversion of glycerol to CH_4 is highly favourable during the reforming process. Thus, the catalyst selected should have sufficient capacity for reforming the produced CH_4 into hydrogen and carbon monoxide, and the catalyst should also facilitate the water gas shift reaction to convert CO into CO_2 providing additional H_2 production. The residence time should be considered as an important parameter for the catalytic reactor. Temperature, gas composition and flow rate must be carefully controlled to obtain high efficiency and avoid catalyst deactivation.

A number of experimental and modelling studies have been carried out to prove the concept of CO_2-sorption enhanced steam reforming by converting methane to H_2.[25, 26] In-situ CO_2 removal is considered to change the normal equilibrium limits of reforming and shift reactions. Thus, hydrogen generation from biomass-derived glycerol using CO_2-sorption enhanced steam reforming will be a promising technology to increase glycerol conversion and H_2 concentration in the product mixture. In addition, it is a lower cost production process of hydrogen based on reducing the number of processing steps required for subsequently separating CO_2.

4. Conclusions

Biodiesel has received considerable attention as an alternate energy source because of its environmental benefits and CO_2 neutral. With increasing biodiesel production, the glycerol by-product is becoming a cheap market product and may become a waste problem. In this paper, the gas-solid flow and H_2 production from steam reforming of glycerol in a fluidised bed reactor has been simulated using CFD method by an additional transport equation with a kinetic term. The results showed that the gas-solid system of the fluidised bed exhibited a more heterogeneous structure, the dense phase developed into a structure characterised by a maximum volume fraction of 0.52, with particles clusters forming and dissolving dynamically. The core-annulus structure showed that in the gas-solid flow, the solid and gas velocities in the core region were much higher than that in the annulus region, while solid and gas velocities near the wall decreased and had a downward component. The bed expansion was about 300%-350% and a considerable pressure fluctuation was observed. The results showed the glycerol conversion and H_2 production increased with increasing the time and most of the gas products of H_2, CO_2, CH_4 and CO were formed during the initial 2 s. The CO_2 in product gases remained considerable amount and thus hydrogen generation from biomass-derived glycerol using CO_2-sorption enhanced steam reforming will be a promising technology achieving high purity H_2 production and CO_2 sequestration. The authors' current work focuses on experimental studies of the latter using both confined fluidised bed and fixed bed technology (papers in preparation).

Nomenclature

$\vec{a}$	acceleration, m/s^2
c	cell
C_D	drag coefficient
D_i	diffusion coefficient for species i in the mixture
e	restitution coefficient
$\vec{F}_g$	drag force, kg.m/s^2
$\vec{g}$	gravity acceleration, m/s^2
g_0	radial distribution function
h_c	particle height, m
$\bar{h}_p$	average particle height, m
J_i	diffusion flux of species i
k_s	diffusion coefficient for granular energy
K_{gs}	interface momentum transfer coefficient
L	height of the bed, m
m	mass, kg
N	number of chemical species
N_k	cell number
n	average molar flow rate, kmol/s
p	thermodynamic pressure, Pa
p_s	solids pressure, Pa
R	universal gas constant, Pa.m^3/kmol.K
Re	Reynolds number
R_i	source of chemical species i due to reaction
t	time, s
$\vec{v}$	velocity, m/s

X_i	local mass fraction of each species
z	unit length, m

Greek letters

ε	phase fraction
ρ	density, kg/m^3
$\vec{\tau}$	stress tensor, Pa
Θ_s	granular temperature, m^2/s^2
μ_s	solids shear viscosity, kg/(s.m)
$\mu_{s.dil}$	solid phase dilute viscosity, kg/(s.m)
λ_s	bulk viscosity, kg/(s.m)
γ_s	collision dissipation of energy, kg/(s^3.m)
ϕ_{gs}	transfer of kinetic energy, kg/(s^3.m)

Subscripts

g	gas
s	solids
mf	minimum fluidisation

References

(1) Valliyappan, T.; Bakhshi, N. N.; Dalai, A. K. Pyrolysis of glycerol for the production of hydrogen or syn gas. Bioresource Technology 2008, 99, 4476-4483.

(2) Kunii, D.; Levenspiel, O. Fluidization Engineering. Butterworth-Heinemann Series in chemical engineering. Editor: Brenner H. MA, 1991.

(3) Gidaspow, D. Multiphase Flow and Fluidization, Continuum and Kinetic Theory Description, Academic Press, NY, 1994.

(4) Chaouki, J.; Gonzalez, A.; Guy, C.; Klvana, D. Two-phase model for a catalytic turbulent fluidized-bed reactor: Application to ethylene synthesis. Chemical

Engineering Science 1999, 54, 2039-2045.

(5) Zou, L.M.; Guo, Y. C.; Chan, C. K. Cluster-based drag coefficient model for simulating gas–solid flow in a fast-fluidized bed. Chemical Engineering Science 2008, 63, 1052-1061.

(6) Ahmadzadeh, A.; Arastoopour, H.; Teymour, F. Numerical simulation of gas and particle flow in a rotating fluidized bed. Ind. Eng. Chem. Res. 2003, 42, 2627-2633.

(7) Jiradilok, V.; Gidaspow, D.; Breault, R. W. Computation of gas and solid dispersion coefficients in turbulent risers and bubbling beds. Chemical Engineering Science 2007, 62, 3397-3409.

(8) Qi, H.Y.; Li, F.; Xi, B.; You, C. F. Modeling of drag with the Eulerian approach and EMMS theory for heterogeneous dense gas-solid two-phase flow. Chemical Engineering Science 2007, 62, 1670-1681.

(9) Sun, J.; Battaglia, F. Hydrodynamic modeling of particle rotation for segregation in bubbling gas-fluidized beds. Chemical Engineering Science 2006, 61, 1470-1479.

(10) Lettieri, P.; Felice, R. D.; Pacciani, R.; Owoyemi, O. CFD modeling of liquid fluidized beds in slugging mode. Powder Technology 2006, 167, 94-103.

(11) Benyahia, S.; Arastoopour, H.; Knowlton, T. M.; Massah, H. Simulation of particles and gas flow behavior in the riser section of a circulating fluidized bed using the kinetic theory approach for the particulate phase, Powder Technology 2000, 112, 24-33.

(12) Therdthianwong, A.; Pantaraks, P.; Therdthianwong, S. Modeling and simulation of circulating fluidized bed reactor with catalytic ozone decomposition reaction. Powder Technology 2003, 133, 1-14.

(13) Zimmermann, S.; Taghipour, F. CFD Modeling of the hydrodynamics and Reaction Kinetics of FCC Fluidized-Bed Reactors. Ind. Eng. Chem. Res. 2005, 44,

9818-9827.

(14) He, Y. R.; Lu, H. L.; Sun, Q. Q.; Yang, L. D.; Zhao Y. H.; Gidaspow, D.; Bouillard, J. Hydrodynamics of gas-solid flow around immersed tubes in bubbling fluidized beds. Powder Technology 2004, 145, 88-105.

(15) Yin B.; Zhang M. C.; Dou B. L.; Song, Y. B.; Wu, J. Discrete particle simulation and visualized research of gas-solid flow in an internally circulating fluidized bed. Ind Eng Chem Res. 2003, 42, 214-221.

(16) FLUENT Inc. FLUENT 6.0 User's Guide; FLUENT Inc.: Lebanon, NH, 2001.

(17) Lu, H.; Gidaspow, D.; Bouillard, J.; Liu, W. Hydrodynamic simulation of gas-solid flow in a riser using kinetic theory of granular flow. Chemical Engineering Journal 2003, 95, 1-13.

(18) Sotudeh-Gharebagh, R.; Mostoufi, R. Simulation of a catalytic turbulent fluidized bed reactor using the sequential modular approach. Fuel Processing Technology 2003, 85, 189-200.

(19) Dauenhauer, P. J.; Salge, J. R.; Schmidt, L. D. Renewable hydrogen by autothermal steam reforming of volatile carbohydrates. Journal of Catalysis 2006, 244 238-247.

(20) Adhikari, S.; Fernando, S.; Gwaltney, S. R.; To, S. D.; Bricka, R. M.; Steele, P. H.; Haryanto, A. Athermodynamic analysis of hydrogen production by steam reforming of glycerol. International Journal of Hydrogen Energy 2007, 32, 2875-2880.

(21) Zhang, B.; Tang, X.; Li, Y.; Xu, Y.; Shen, W. Hydrogen production from steam reforming of ethanol and glycerol over ceria-supported metal catalysts. International Journal of Hydrogen Energy 2007, 32, 2367-2373.

(22) Gungor, A.; Eskin, N. Hydrodynamic modelling of a circulating fluidized bed.

Powder Technology 2007, 172, 1-13.

(23) Adhikari, S.; Fernando, S. D.; To, S. D. F.; Bricka, R. M.; Steele, P. H.; Haryanto, A. Conversion of Glycerol to Hydrogen via a Steam Reforming Process over Nickel Catalysts. Energy & Fuels 2008, 22, 1220-1226.

(24) Dupont, V.; Ross, A. B.; Hanley, I.; Twigg, M. V. Unmixed steam reforming of methane and sunflower oil: a single reactor process for H_2-rich gas. International Journal of Hydrogen Energy 2007, 32, 67-79.

(25) Ding, Y.; Alpay, E. Adsorption-enhanced steam methane reforming. Chemical Engineering Science 2000, 55, 3929-3940.

(26) Barelli, L.; Bidini, G.; Gallorini, F.; Servili. S. Hydrogen production through sorption-enhanced steam methane reforming and membrane technology: A review. Energy 2008, 33, 554-570.

Table 1. Parameters for the simulation

Gas phase	Glycerol, steam and N_2
Inlet gas components	Glycerol: 1.10×10^{-3} kmol/m^3; Steam: 6.22×10^{-3} kmol/m^3: N_2: 3.24×10^{-2} kmol/m^3
Inlet gas velocity	0.5 m/s
Gas density	volume-weighted-mixing-law
Gas bulk viscosity	0.172 cP
Outlet pressure	101325 Pa
Solid phase	sand and Ni-based catalyst
Particle shape	sphere
Particle size	8.75×10^{-5} m
Particle density	2650 kg/m^3
Coefficient of restitution	0.95
Initial solid fraction	0.52
Reaction	laminar finite rate model

Fig.1. Two-dimensional computational domain.

0s   0.5s   1.0s   1.5s   2.0s   2.5s   3.0s   3.5s   4.0s
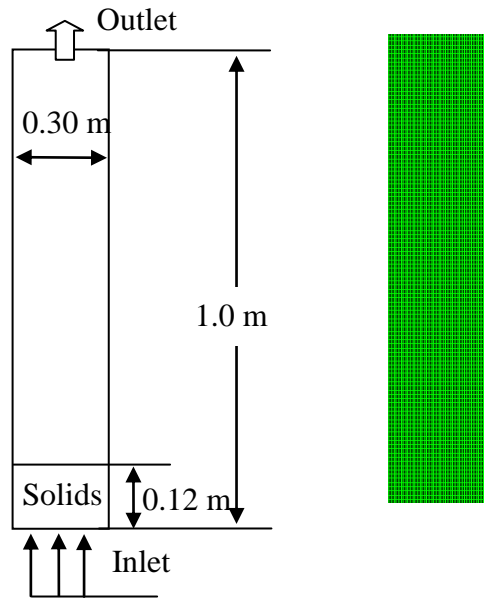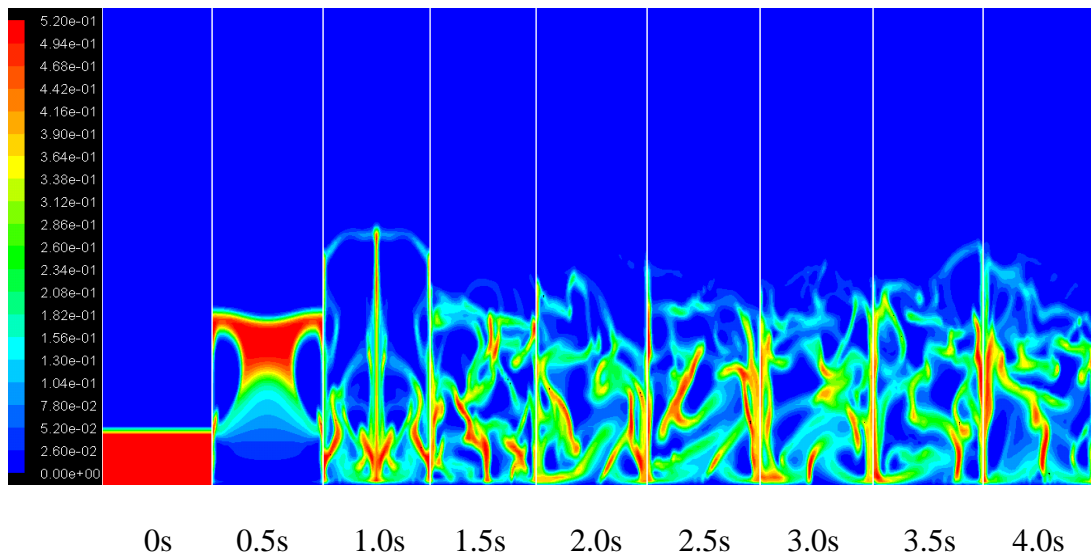
Fig. 2. Solids volume fraction at different times.
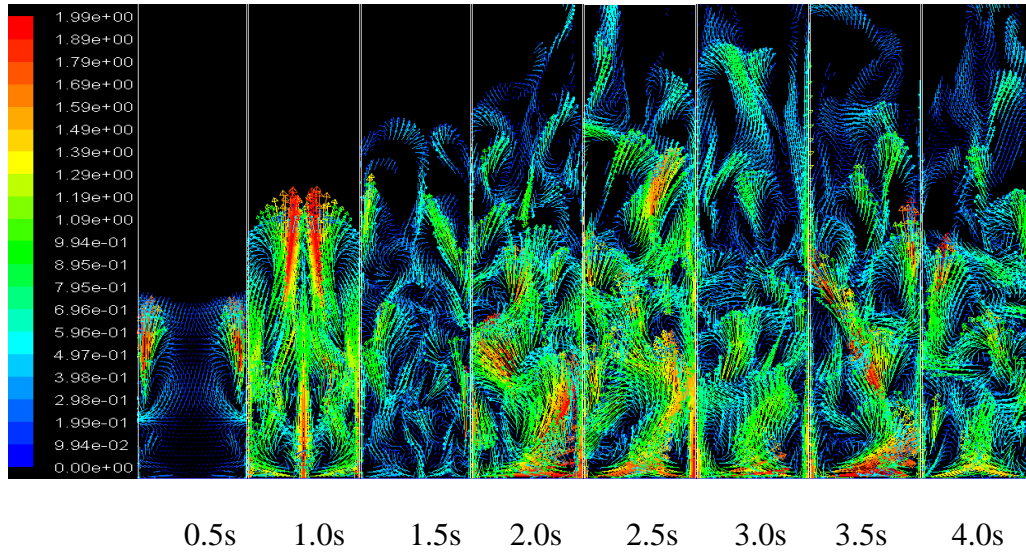
Fig. 3. Solids velocity vector plots, velocity coloured by velocity magnitude, m/s.
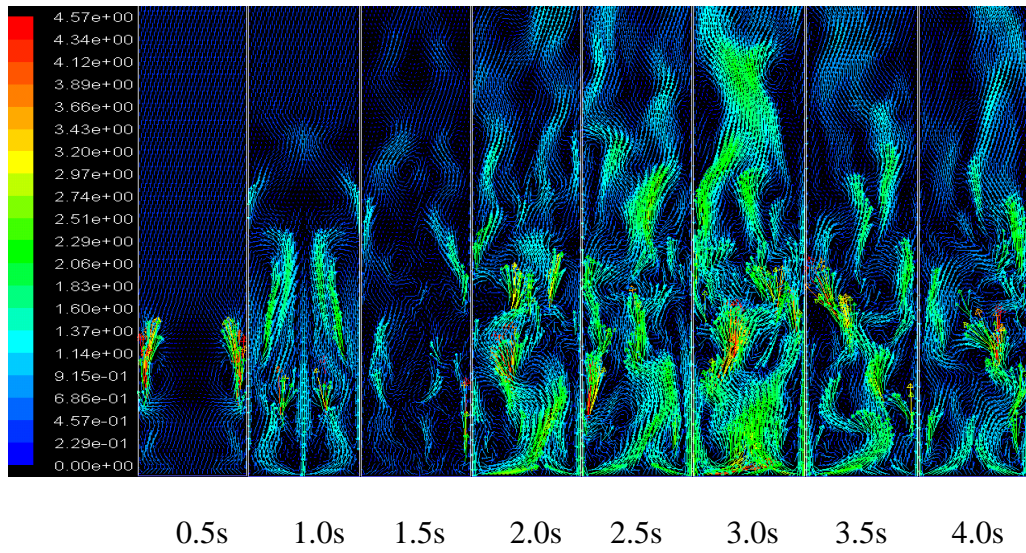
Fig. 4. Gases velocity vector plots, velocity coloured by velocity magnitude, m/s.
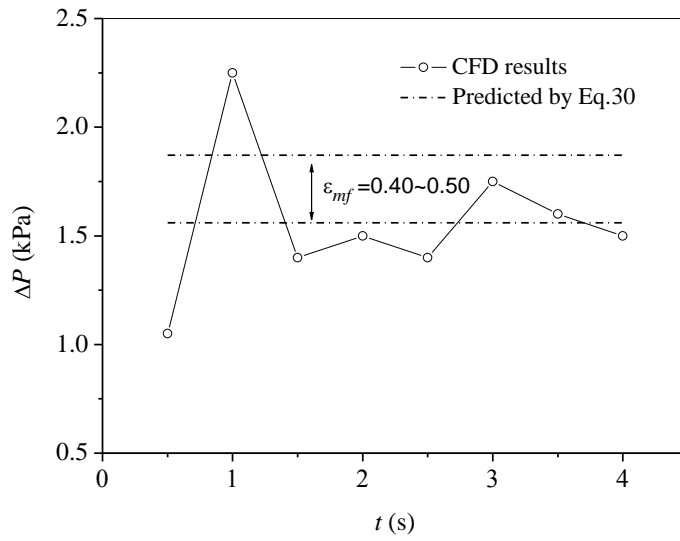
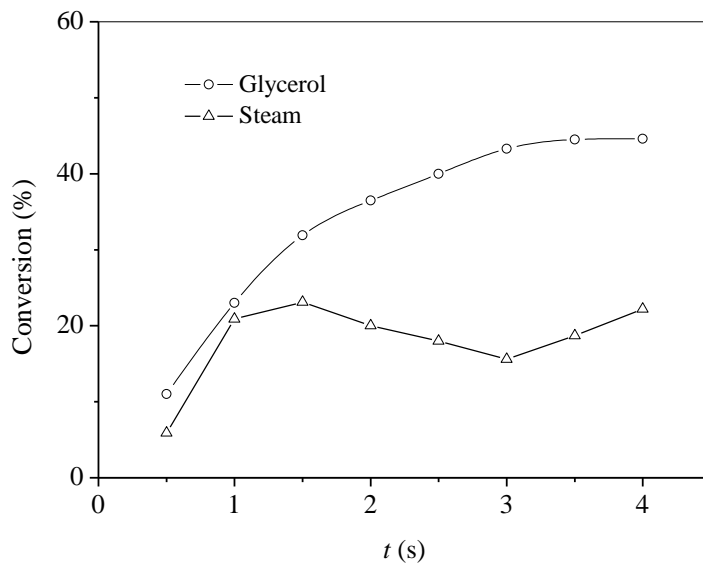**Fig. 5. Pressure drop across the bed in initial time of 4 s.**
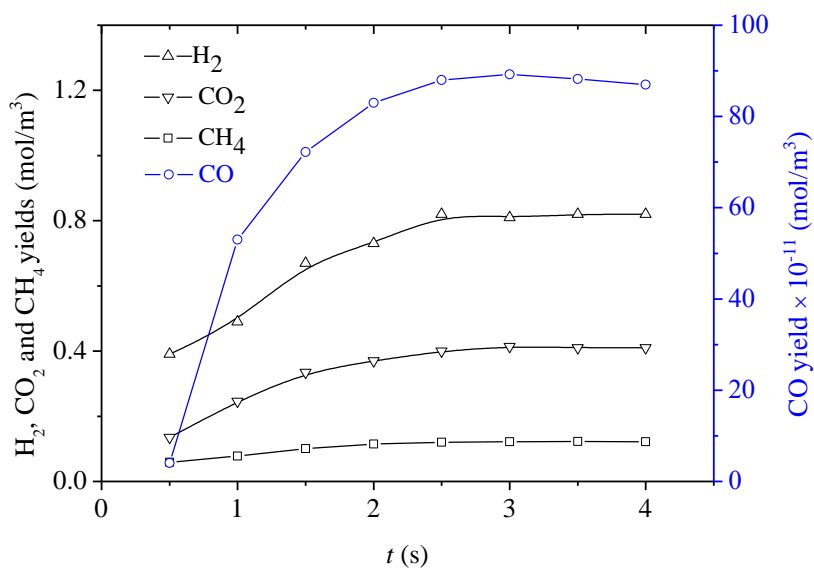

Fig. 6. Conversions of glycerol and steam (%).
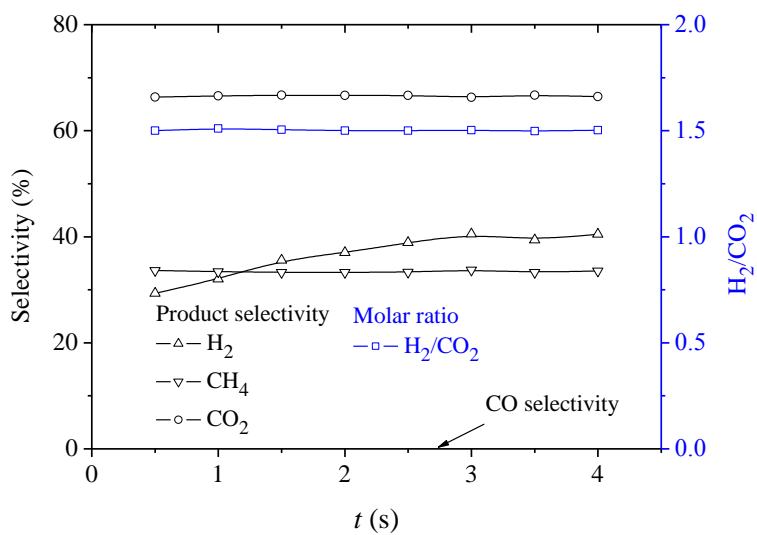
Fig. 7. Concentrations of gaseous products (mol m^{-3}).

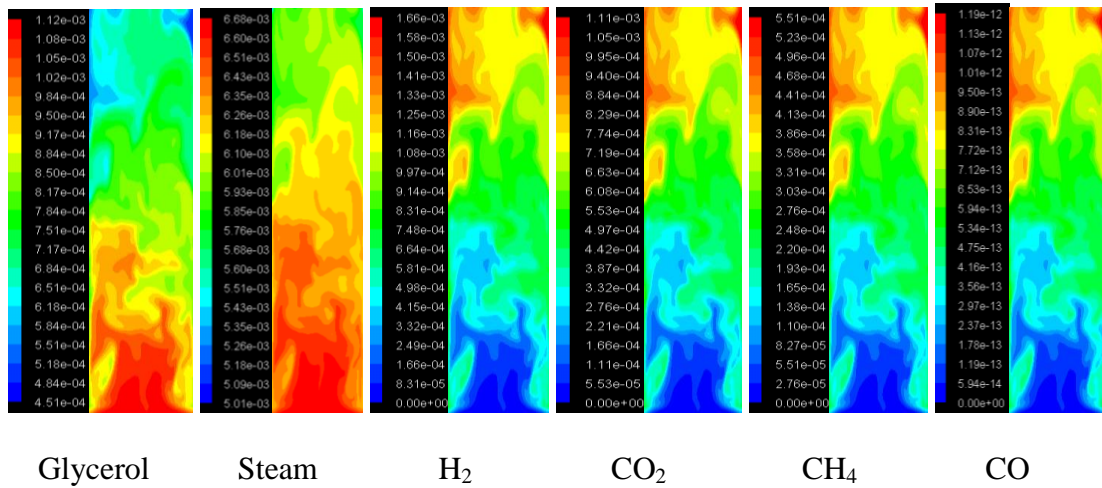**Fig. 8. Product selectivity and the molar ratio of H$_2$/CO$_2$.**

| Glycerol | Steam | H$_2$ | CO$_2$ | CH$_4$ | CO |

Fig. 9. Concentration distributions of glycerol, steam and gaseous products at 4 s, kmol/m^3.
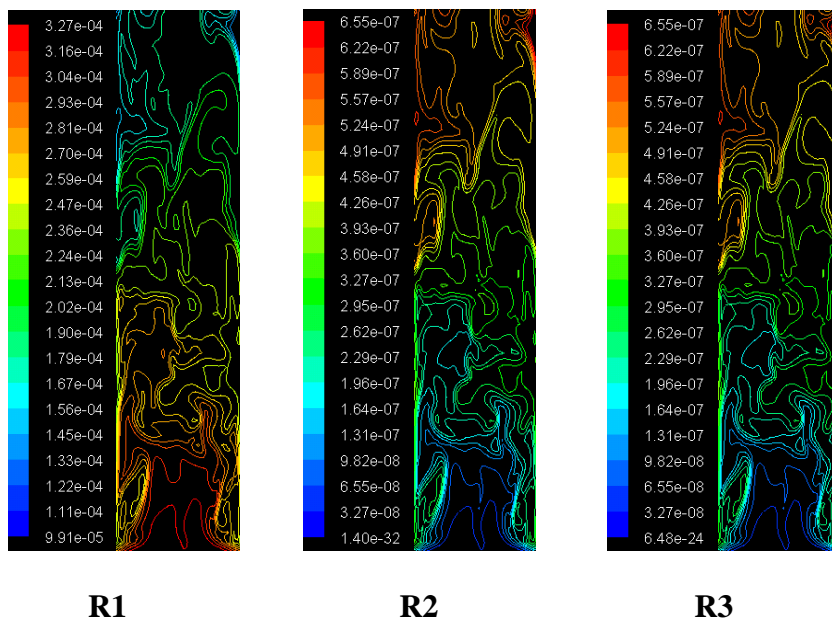

| **R1** | **R2** | **R3** |

Fig. 10. Arrhenius rates of three chemical reactions at 4 s, kmol/m^3·s.